

COMPUTATIONAL AND EXPERIMENTAL STUDY OF AMMONIUM PERCHLORATE/ETHYLENE COUNTERFLOW DIFFUSION FLAMES

M. D. SMOOKE,¹ R. A. YETTER,² T. P. PARR,³ D. M. HANSON-PARR,³ M. A. TANOFF,⁴
M. B. COLKET⁵ AND R. J. HALL⁵

¹*Department of Mechanical Engineering
Yale University*

New Haven, CT 06520-8284, USA

²*Department of Mechanical and Nuclear Engineering
The Pennsylvania State University
University Park, PA 16802, USA*

³*Weapons Division
Naval Air Warfare Center
China Lake, CA 93555-6100, USA*

⁴*W. K. Kellogg Institute
Battle Creek, MI 49016-3232, USA*

⁵*United Technologies Research Center
East Hartford, CT 06108, USA*

We investigated the modeling of counterflow diffusion flames in which the products of ammonium perchlorate (AP) combustion were counterflowed against an ethylene fuel stream. The two-dimensional problem can be reduced to a one-dimensional boundary value problem along the stagnation point streamline through the introduction of a similarity transformation. By utilizing recent developments in hydrocarbon, chlorine, NO_x and AP kinetics, we formulated a detailed transport, finite-rate chemistry system for the temperature, velocity, and species mass fractions of the combined flame system. A detailed soot model is included which can predict soot volume fractions as a function of the strain rate and the fuel mole fraction. We compare the results of this model with a series of experimental measurements in which the temperature was measured with radiation-corrected thermocouples and OH rotational population distribution; several important species were measured with planar laser-induced fluorescence, UV-visible absorption, and Raman spectroscopies; and the soot volume fraction was measured with laser-induced incandescence and visible absorption spectroscopy.

Introduction

Many solid rocket propellants are based on a composite mixture of ammonium perchlorate (AP) oxidizer and polymeric binder fuels. In these propellants, complex three-dimensional diffusion flame structures between the AP and binder decomposition products, dependent upon the length scales of the heterogeneous mixture, drive the combustion via heat transfer back to the surface. Changing the AP crystal size changes the burn rate of such propellants. Large AP crystals are governed by the cooler AP self-deflagration flame and burn slowly, while small AP crystals are influenced more by the hot diffusion flame with the binder and burn faster. This allows control of composite propellant ballistic properties via particle size variation.

Previous measurements on AP/binder diffusion flames in a planar two-dimensional sandwich configuration have yielded insight into the controlling flame structure [1,2], but there are several drawbacks that make comparison with modeling difficult.

First, the flames are two-dimensional in structure, making modeling much more complex computationally than with one-dimensional propellant systems, such as cyclotrimethylene trinitramine (RDX) self- and laser-supported deflagration [3]. In addition, little is known about the nature, concentration, and evolution rates of the gaseous chemical species produced by the various binders as they decompose. This makes comparison with models quite difficult. Alternatively, counterflow flames provide an excellent geometric configuration within which AP/binder diffusion flames can be studied both experimentally and computationally.

While counterflow diffusion flames have been studied in recent years using experimental, theoretical, and numerical techniques [4–10], there has been little work in which these tools have been applied to the study of solid propellants in this configuration. While some preliminary studies of AP counterflow flames were made by Friedman [11], Ablow and Wise [12], Inami and Wise [13], Wiersma and

Report Documentation Page

Form Approved
OMB No. 0704-0188

Public reporting burden for the collection of information is estimated to average 1 hour per response, including the time for reviewing instructions, searching existing data sources, gathering and maintaining the data needed, and completing and reviewing the collection of information. Send comments regarding this burden estimate or any other aspect of this collection of information, including suggestions for reducing this burden, to Washington Headquarters Services, Directorate for Information Operations and Reports, 1215 Jefferson Davis Highway, Suite 1204, Arlington VA 22202-4302. Respondents should be aware that notwithstanding any other provision of law, no person shall be subject to a penalty for failing to comply with a collection of information if it does not display a currently valid OMB control number.

1. REPORT DATE 04 AUG 2000	2. REPORT TYPE N/A	3. DATES COVERED -	
4. TITLE AND SUBTITLE Computational and Experimental Study of Ammonium Perchlorate/Ethylene Counterflow Diffusion Flames		5a. CONTRACT NUMBER	
		5b. GRANT NUMBER	
		5c. PROGRAM ELEMENT NUMBER	
6. AUTHOR(S)		5d. PROJECT NUMBER	
		5e. TASK NUMBER	
		5f. WORK UNIT NUMBER	
7. PERFORMING ORGANIZATION NAME(S) AND ADDRESS(ES) 1Department of Mechanical Engineering Yale University New Haven, CT 06520-8284, USA		8. PERFORMING ORGANIZATION REPORT NUMBER	
9. SPONSORING/MONITORING AGENCY NAME(S) AND ADDRESS(ES)		10. SPONSOR/MONITOR'S ACRONYM(S)	
		11. SPONSOR/MONITOR'S REPORT NUMBER(S)	
12. DISTRIBUTION/AVAILABILITY STATEMENT Approved for public release, distribution unlimited			
13. SUPPLEMENTARY NOTES See also ADM001790, Proceedings of the Combustion Institute, Volume 28. Held in Edinburgh, Scotland on 30 July-4 August 2000. , The original document contains color images.			
14. ABSTRACT			
15. SUBJECT TERMS			
16. SECURITY CLASSIFICATION OF:			17. LIMITATION OF ABSTRACT
a. REPORT unclassified	b. ABSTRACT unclassified	c. THIS PAGE unclassified	UU
			18. NUMBER OF PAGES 8
			19a. NAME OF RESPONSIBLE PERSON

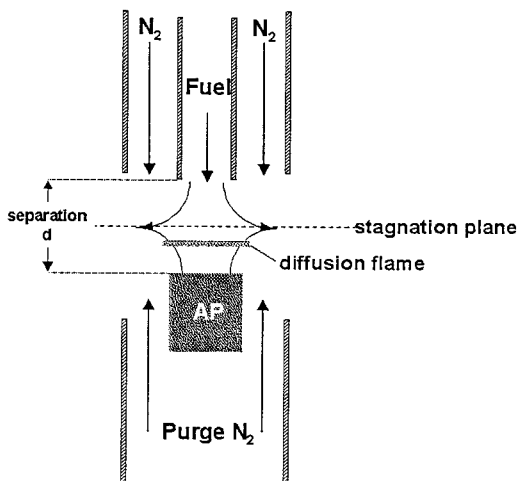


FIG. 1. Schematic of experimental configuration for ethylene versus AP counterflow flame system.

Wise [14], and Mitani and Niioka [15], the first work that combined a detailed transport/finite-rate chemistry model of AP counterflow diffusion flames with experimental measurements was by Tanoff et al. [16]. This study focused on an investigation of counterflow diffusion flames in which the products of AP combustion were counterflowed against a methane fuel stream. By utilizing developments in hydrocarbon, chlorine, NO_x and AP kinetics, a detailed transport, finite-rate chemistry system for the temperature, velocity, and species mass fractions of the combined flame system was formulated. Results of the model were compared with a series of experimental measurements.

In this paper, we continue our investigation of AP counterflow diffusion flames by incorporating two major modifications into the model developed in Ref. [16]. First, the fuel was replaced by ethylene, and second, a detailed soot model was included in the problem. Ethylene is an important reaction intermediate of hydrocarbon binders, and thus, the understanding of this system represents an essential hierarchical step toward the detailed analysis of a composite propellant. Because composite propellant formulations are overall fuel-rich and heterogeneous, soot formation and its coupling to energy release rates and radiative feedback to the surface are fundamental processes that directly impact propellant performance and design. An accurate soot model is therefore a necessary submodel for any detailed composite propellant model.

We compare the results of the computational model with a series of experimental measurements in which the temperature was measured with radiation-corrected thermocouples and OH rotational population distribution, several important species

were measured with planar laser-induced fluorescence (PLIF), UV-visible absorption, and Raman spectroscopies, and the soot volume fraction was measured with laser-induced incandescence (LII) and visible absorption spectroscopy. In the next three sections, the experimental and computational approaches and the kinetic mechanism are outlined, after which the results are presented and discussed.

Experimental Approach

In a typical counterflow diffusion flame experiment, two laminar plug flow jets (one fuel and one oxidizer) are directed toward each other and impinge in the middle of the domain. Properly designed, this configuration leads to a one-dimensional flame along the stagnation point streamline that can be modeled as a one-dimensional problem. In addition, the experimentalist has complete control over many flame parameters including fuel chemistry, fuel thermal properties (via dilution, for example), and flame strain rate. In our case, the oxidizer side was not a jet but a solid pellet of AP. Although AP does not normally self-deflagrate at pressures below 200 to 800 psia (depending on purity), it was found that the counterflow diffusion flame was self-sustaining even at 1 atm, and that nearly perfect planar multiflame structures were imaged with methane and ethylene as fuels. Fuel mixtures can be selected to simulate the decomposition products of various binders, or a single fuel can be selected to better understand the kinetics involved.

The flame configuration is illustrated in Fig. 1. The fuel exit diameter was 7.75 mm, and the AP pellet diameter was 10.1 mm. Both the AP and fuel flows were surrounded by nitrogen shroud flows (26.8 mm diameter for the fuel and 23.0 mm for the AP). The shroud flows were set to match the fuel and AP decomposition gas flows. The fuel flow rate was controlled with a calibrated flow meter, but the AP decomposition gas flow rate was determined by the AP solid regression rate. The AP pellet and the ethylene jet were separated by 5.0 mm, with an ethylene average flow speed of 20.5 cm/s, yielding an AP regression rate of 0.113 mm/s and a corresponding strain rate of approximately 311 s^{-1} . The AP surface location was maintained with a mechanical stage that offset the regression rate. The AP was ultrahigh purity (UHP) grade from Kerr McGee Corporation, pressed to 98.2% theoretical maximum density (TMD). UHP AP was used because the flame structure and even the regression rate are sensitive to impurities in normal research-grade AP.

Diagnostics applied to the counterflow AP diffusion flame included radiation-corrected thermocouples and OH rotational measurements for the temperature, PLIF imaging for OH, CN, and NO species profiles, Raman spectroscopy for absolute

major species profiles, and LII for the soot volume fraction. UV-visible absorption spectroscopy was used to obtain absolute number densities for the OH and NO, and for the soot volume fraction. The CN concentration was below the CN absorption spectroscopy detection limit of approximately 5–10 ppm. The CN radicals were monitored with PLIF by pumping the (0,0) bandhead of the B-X transition near 388.3 nm while monitoring (0,1) emission around 422 nm.

On the fuel side, where OH temperature measurements were not feasible, 50 μm thermocouples were used to measure the temperature distribution. The AP-side temperature was obtained from OH PLIF measurements of the R1(3), R1(10), and R1(14) lines of the (1,0) A-X OH transition. The temperature was then obtained from a Boltzmann distribution plot.

The NO profile shape was obtained via PLIF by pumping selected rotational lines (R2(7), Q₂ + Q₁₂(10), and P₂ + P₁₂(16) at 236.639 nm of the (0,1) hot band of the A-X gamma system), while monitoring (0,3) emission around 260 nm. The profile shape was corrected for the temperature dependence of these ro-vibrational lines using the measured temperature profile. The NO vibrational temperatures obtained from the absorption spectral fits (to give absolute concentration in mole fraction) matched the measured OH rotational temperature.

Major species such as C₂H₄, O₂, HCl, CO, H₂, and H₂O were measured by Raman spectroscopy using 330 mJ of 532 nm light from a Nd:YAG laser (see also Ref. [16]). The Raman signal was focused onto a 0.22 m focal length spectrograph and optical multichannel analyzer. Two spectra were obtained for each experiment: one with vertical laser polarization and one with horizontal. All of the major Raman lines monitored disappear when observed along the polarization vector, while interfering signals, such as laser induced fluorescence (LIF), are not affected. Thus, the interference is removed by subtracting the horizontal polarization signal from the vertical. The major interference comes from C₂ Swan band LIF, which does not occur in the spectral regions for the monitored Raman lines and occurs only in limited spatial regions of the flame. The Raman signals were averaged over time, between 5 and 30 s, to build up reasonable statistics. (In the hot regions of the flame, the number density was so low that collected Raman signals were as low as a few counts per second).

LII measurements were made for the AP/ethylene system to obtain soot volume fraction and size profiles. LII is a result of laser heating of particulates which then radiate broadband. The setup for these measurements was the same as for PLIF, but the laser was tuned off-resonance for molecular transitions, and the narrowband optical collection filter was replaced with a broadband filter to collect more blackbody incandescence. The particle size was also

obtained from the time dependence of the LII emission [17]. A Gaussian-like growth and decay curve was obtained with maximum particle diameters of approximately 50 nm.

The soot profile was made absolute by using results from line-of-sight extinction measurements [18]. A CW diode pumped Nd:YAG laser of wavelength 532 nm was split into two beams, one of which was monitored as the unattenuated beam (I_0) and the other of which passed through the flame. This latter beam was attenuated through extinction by soot particles. The ratio of attenuated (I) to unattenuated light (I_0), or the transmission (I/I_0), was measured with photodiodes. Since the particle diameters were in the nanometer size range, the Rayleigh limit [19] was valid for the computations in converting measured transmission to soot volume fraction. The soot volume fraction (f_v) was obtained from the following formula [19]:

$$f_v = -(\lambda/K_a) \ln(I/I_0)/L \quad (1)$$

where L is the pathlength (in cm) over which attenuation took place, λ is the laser wavelength (cm), and K_a is the absorption coefficient. In the Rayleigh limit, K_a is given by the following [19]:

$$K_a = \frac{(36\pi n^2 \kappa)}{[(n^2(1 - \kappa^2) + 2)]^2 + 4n^4 \kappa^2} \quad (2)$$

where n is the real part and $n\kappa$ is the imaginary part of the index of refraction. The index of refraction for soot at 532 nm was obtained from Ref. [19]. Thus, for these experiments, $f_v = -14.7 \ln(I/I_0)/\text{pathlength}$ in parts per million.

For AP/ethylene flames, we noticed that f_v was lower in the central region of the flame than on the edges, due to a radial dependence of the strain rate. Radially offset transmission measurements were made. The data were too noisy for an Abel deconvolution, so a function was assumed for the radial dependence of soot volume fraction, and this was integrated over the line of sight and compared with the measurements; then the functional parameters were adjusted for the best least-squares fit. The soot volume fraction distribution obtained had a minimum on the centerline and increased with increasing radius. The soot volume fraction value used to normalize the LII profile was then an average of the recovered radial distribution over the soot disk area.

Computational Approach

To model the AP/ethylene flame system, we consider a laminar reacting flow stabilized in the vicinity of the stagnation plane between two axisymmetric, counterflowing streams. One stream contains ethylene and the other the AP decomposition products as determined in Ref. [20]. The complete formulation of the mathematical model for solving the finite

TABLE 1
AP Surface Species (mole fractions)

Species	X_k
O ₂	0.22
N ₂	0.03
H ₂ O	0.38
HCl	0.09
NH ₃	0.08
NO ₂	0.06
N ₂ O	0.03
ClO	0.03
Cl ₂	0.03
ClO ₂	0.02
HClO ₄	0.02
NO	0.01

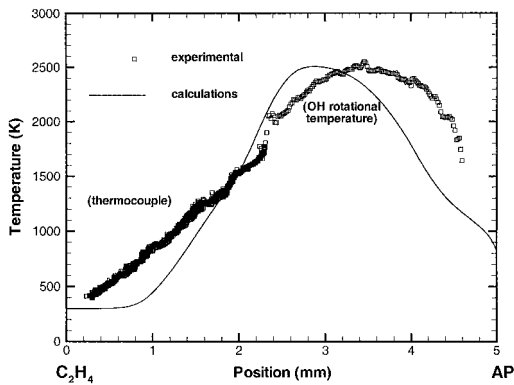


FIG. 2. Comparison between experimentally measured and calculated temperature profiles for the ethylene versus AP counterflow flame.

burner separation problem with plug flow boundary conditions [21,22] starts with the elliptic form, in cylindrical coordinates, of the two-dimensional equations describing the conservation of total mass, individual chemical species mass, momentum, and energy for the reactive flow occurring between the fuel and the AP solid. By seeking a similarity solution of the governing equations, we can reduce the problem to the solution of a nonlinear, two-point boundary value problem in the axial direction along the stagnation point streamline.

Soot kinetics were modeled as coalescing, solid carbon spheroids undergoing surface growth in the free molecule limit. The particle mass range of interest was divided into sections [23], and an equation was written for each section, including coalescence, surface growth, and oxidation. Sectional analysis makes it possible to obtain the particle size distribution without *a priori* assumptions about the form

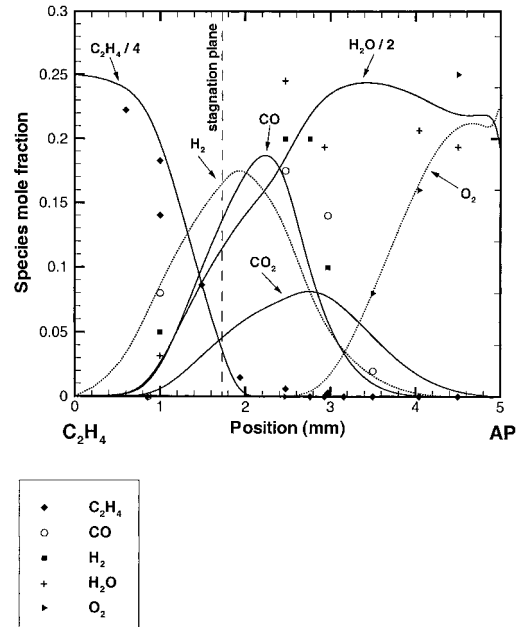


FIG. 3. Comparison between experimentally measured and computed major species profiles for the ethylene versus AP counterflow flame.

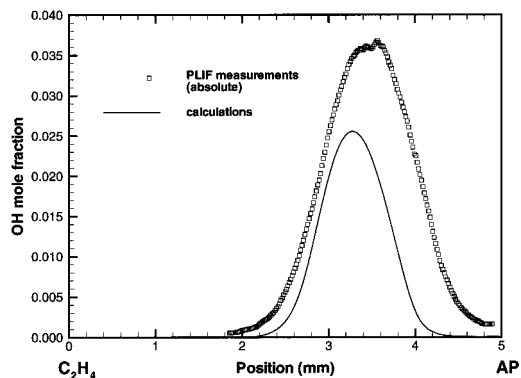


FIG. 4. Comparison between experimentally measured (PLIF) and calculated OH concentration profiles for the ethylene versus AP counterflow flame. Experimental OH measurements are absolute concentrations.

of the distribution. For the smallest section, an inception source term was included. The transport conservation equation for each section includes thermophoresis, an effective bin diffusion rate, and source terms for gas-phase scrubbing. The gas and soot equations are additionally coupled through non-adiabatic radiative loss in the optically thin approximation. The inception model employed here is

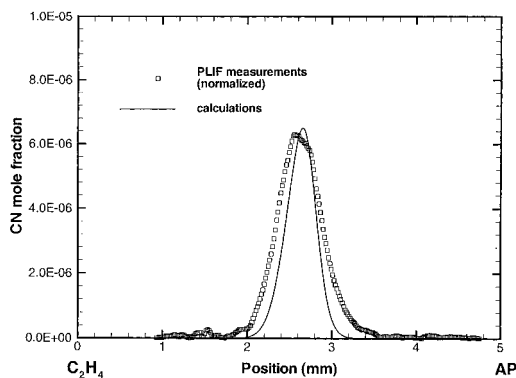


FIG. 5. Comparison between experimentally measured (PLIF) and calculated CN concentration profiles for the ethylene versus AP counterflow flame. Experimental CN measurements have been normalized to the peak concentration predicted by the model, but the spatial positions are absolute.

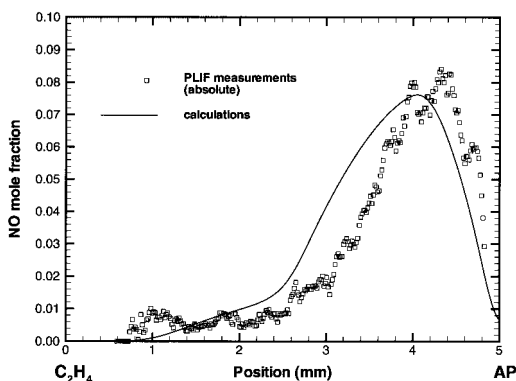


FIG. 6. Comparison between experimentally measured (PLIF) and calculated NO concentration profiles for the ethylene versus AP counterflow flame. Experimental NO measurements are absolute concentrations.

based on an estimate of the formation rate of two- and three-ringed aromatic species (naphthalene and phenanthrene) and is a function of local acetylene, benzene, phenyl, and molecular hydrogen concentrations [24]. The contributions from the inception processes were incorporated in the first sectional bin, whose lower mass boundary was set equal to the mass of the smallest inception species (127 amu). In the sectional representation [23], the sectional mass boundaries varied linearly on a logarithmic scale. The number of sections required for convergence must be examined for each problem and depends on the relative magnitudes of surface growth and inception. Oxidation of soot by O_2 and OH was treated as described in Ref. [25]. The surface growth rate was that proposed by Colket and Hall (denoted by

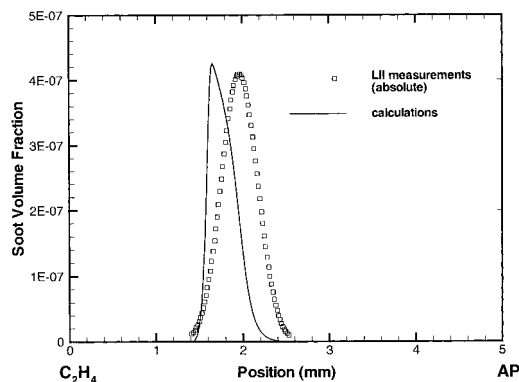


FIG. 7. Comparison between experimentally measured (LII) and calculated soot volume fraction profiles for the ethylene versus AP counterflow flame. Experimental soot measurements are absolute soot volume fractions.

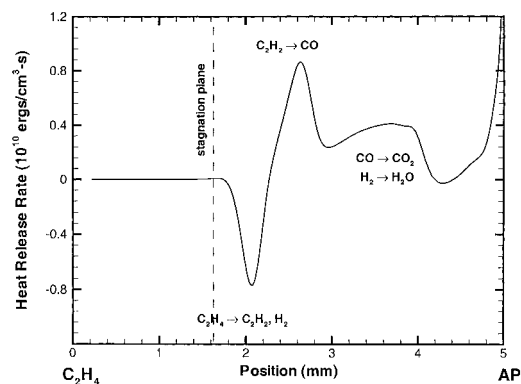


FIG. 8. Computed heat release rate profile for the ethylene versus AP counterflow flame.

MODFW in Ref. [26]). The mechanism treated both acetylene addition and elimination, and hence simulates the rapid fall-off of surface growth rates at elevated temperatures. Use of an expression with a simple Arrhenius form results in a gross overprediction of soot in these flames.

The governing equations were discretized with an adaptive finite difference algorithm and solved using Newton's method for the velocities, the temperature, the gas-phase species, and the particle sectional mass fractions. The system was closed with the ideal gas law, and appropriate boundary conditions were applied on each side of the computational domain. Local properties were evaluated using vectorized and highly optimized transport and chemistry libraries [27]. The sectional thermophoretic velocities in the free molecule regime were given in Ref. [25], as were the sectional diffusion velocities, which were

written with a mass-weighted mean diffusion coefficient for each size class. In the optically thin radiation model used in our calculations, the significant radiating species, in addition to particulates, were H_2O , CO , and CO_2 . Given the length scales of the flame investigated, it is highly unlikely that self-absorption was important. Although the soot volume fraction reached parts per million levels, the narrowness of the soot shell (1–2 mm) mitigated any self-absorption effects. We utilize temperature, species [20], and regression rate (velocity) information from the experiments for both the AP and the ethylene fuel jet boundary conditions.

Results

In this section we examine the flame structure of a one-dimensional AP/ethylene counterflow diffusion flame. Pure ethylene flowed from the fuel jet at 298 K with a velocity of 20.5 cm/s. The AP surface was maintained at its 1 atm decomposition temperature of 825 K. The species that emerged from the AP surface are listed in Table 1 [20]. They had a flow speed of 47.8 cm/s, which corresponds to an AP regression rate of 0.113 mm/s (solid density = 1.975 g/cm³). Computations were performed with a reaction mechanism that combined the mechanism utilized in Ref. [16] with the ethylene and benzene chemistry employed in Ref. [28]. The complete mechanism contains a total of 105 chemical species participating in 660 reversible chemical reactions. Twenty soot classes were included in the computation.

The model predicts an AP decomposition flame above the AP surface, followed by an ethylene/AP-products diffusion flame, in agreement with experimental observations of the OH and CN profiles. Both flame structures lie to the AP side of the stagnation plane, which occurs at 1.73 mm above the ethylene burner. The stagnation plane is located on the fuel-rich side of the ethylene/air diffusion flame.

The AP/ethylene system is remarkably rich in structure. Color imaging shows four distinct flame regions [29]. Near the AP surface is an orange region containing the burned gases of the AP self-deflagration flame, which has an extremely short standoff distance (<50 μm). The second region, which is light blue in color, is where OH radicals first start to appear. This region is followed by a third zone which is reddish purple in color and contains the primary diffusion flame with high radical concentrations. Finally, as one moves toward the ethylene jet, a bright yellowish region appears in the fuel-rich side of the diffusion flame, indicating the presence of soot.

A comparison between the computed and measured temperature profiles in Fig. 2 illustrates the overall good agreement between the model and the experiments, with the exception of a slight shift between computed and measured profiles and a

steeper slope in the predicted temperature profile on the ethylene side. Both profiles illustrate the extremely rapid rise in the temperature as one moves away from the AP surface, with a slower temperature decrease as the ethylene jet is approached. The rise in the temperature as one moves away from the AP surface is due primarily to the high AP surface temperature and the resulting premixed flame that is formed when HClO_4 and NH_3 burn with oxygen. The temperature rises approximately 1700 K within 2 mm from the AP surface.

Figure 3 shows a plot of comparisons among the computed and experimental major species profiles of the AP/ethylene system. As in hydrocarbon counterflow diffusion flames, there is very little overlap in the fuel and oxygen profiles. The ethylene decreases monotonically until it is totally consumed in the neighborhood of the peak temperature. As the ethylene disappears, significant quantities of H_2O , H_2 , CO , and CO_2 are formed. (Note that the experimental and numerical ethylene and water profiles were divided by four and two, respectively, to fit on the same scale as the other species shown). What is particularly noteworthy is that, while the hydrogen and carbon monoxide concentrations are negligible about 1 mm above the AP surface, the water concentration is non-trivial as one approaches the AP surface. This is attributed to the water vapor coming off the AP surface and the water vapor formed from the premixed ammonia/perchloric acid flame near the AP surface via the reactions $\text{NH}_3 + \text{OH} \rightarrow \text{NH}_2 + \text{H}_2\text{O}$ and $\text{HCl} + \text{OH} \rightarrow \text{H}_2\text{O} + \text{Cl}$. In addition, most surface oxychlorine compounds (ClO_2 , HClO_4) disappear within 0.1–0.2 mm of the AP surface. ClO , while falling rapidly over this interval from its surface concentration of 0.03 mole fraction, remains present at a low level (0.002 mole fraction) for about 0.6–0.8 mm. ClOH persists in a similar fashion.

In Fig. 4 we compare the computed and experimental OH mole fraction profile. The spatial locations of the two peaks are almost identical, and the peak mole fractions agree to within 30%. In Fig. 5, a similar profile is illustrated for CN. The experimental profile peaks within 0.1 mm of the computed result for CN. The experimental profile is moderately wider in half-width compared to the computation. Only relative mole fractions are reported due to the extremely small mole fraction peaks. Fig. 6 compares computed and experimental NO mole fractions, which are remarkable in their agreement. The location of the peak values are shifted by 0.2 mm, but the agreement between the profiles, including the two-tiered structure with steep gradients on the AP side and the gradual decay on the ethylene side, is excellent.

A comparison of the computed and absolute soot volume fraction is illustrated in Fig. 7. The figure indicates that the soot is localized in a very thin region (1 mm) in the fuel-rich portion of the flame.

This is consistent with the visual observations reported in Ref. [29]. Excellent agreement is obtained for the spatial locations of the computed and measured soot volume fractions, as well as the absolute peak heights (0.41 ppm vs. 0.43 ppm). Relative spatial distributions for the separate processes of surface growth, soot inception, and oxidation, as determined from the model, indicate that the soot oxidation rates observable in this flame are attributable to super-equilibrium OH concentrations, consistent with our previous study [24]. Results not illustrated here indicate that the peak soot volume fraction is extremely sensitive to the strain rate of the system. An order of magnitude reduction in the peak soot volume fraction can be obtained by a moderate increase of the strain rate. This is attributed in part to (1) the variation in peak mole fractions of key growth species such as acetylene and benzene as a function of the strain rate, (2) the temperature dependence of the inception and surface growth processes as a function of the strain rate, and (3) the significant decrease in residence time as the strain rate increases.

In Fig. 8, we plot the heat release rate profile given by

$$\dot{q} = \sum_{k=1}^K h_k \dot{\omega}_k W_k, \quad (3)$$

where h_k denotes the enthalpy of formation of the k th species, $\dot{\omega}_k$ denotes the molar chemical production (destruction) rate of the k th species, and W_k denotes the molecular weight of the k th species. We note four distinct features as one moves from the ethylene jet to the AP surface. First, at approximately 3.0 mm from the AP surface, there is an endothermic region due to the pyrolysis of C_2H_4 to C_2H_2 . This region also corresponds to where the soot surface growth rate is a maximum. Immediately thereafter, the heat release peak has a local maximum due to the consumption of C_2H_2 and the formation of CO. A broad exothermic peak centered at about 1.3 mm above the AP surface results from the conversion of CO to CO_2 and H_2 to H_2O . The overall maximum heat release rate occurs just above the AP surface and is due to the highly exothermic decomposition of $HClO_4$, ClO_3 , and ClO_2 and formation of HCl.

Conclusions

The counterflow geometry has been demonstrated as a well-suited configuration, both experimentally and computationally, for studying the structure of AP propellant deflagrations at atmospheric pressure. Non-intrusive laser diagnostic techniques have proven to be an accurate, reliable means for probing the counterflow flame system's structure, even over relatively small (5 mm) separation distances. The

computationally efficient one-dimensional flame model, with an appropriate kinetics model, has proven to be capable of predicting all of the experimentally observed features of the AP versus ethylene counterflow flame system, including absolute concentrations and structures of NO and OH, the complex spatial activity of NO, CN, OH, the soot volume fraction, and the temperature profile throughout both the AP decomposition flame (above the AP surface) and the ethylene/AP-products diffusion flame. A detailed soot model reveals a high-sooting region in the fuel-rich region of the flame. This is supported by experimental LII measurements. Analysis of the computed heat release profile reveals a multistage set of reaction zones, consistent with color imaging performed experimentally. The results of this study show that the counterflow geometry provides an excellent configuration in which to study propellant oxidizer/binder interactions. In future work, we will consider systems in which the decomposition products of hydroxy terminated polybutadiene are used as the fuel.

Acknowledgments

The authors greatly acknowledge Dr. J. Goldwasser of the Office of Naval Research, Dr. R. Miller, formerly of the Office of Naval Research, Dr. J. Tishkoff of the Air Force Office of Scientific Research and Dr. M. King of NASA for partially funding this work.

REFERENCES

- Parr, T. P., and Hanson-Parr, D. M., "AP Diffusion Flame Structure," in *Proceedings of the Thirty-Third JANNAF Combustion Subcommittee Meeting*, Monterey, CA, November 1996, Vol. II, CPIA Publication 653, p. 35.
- Parr, T. P., and Hanson-Parr, D. M., *Proc. Combust. Inst.* 26:1981 (1997).
- Prasad, K., Yetter, R., and Smooke, M. D., *Combust. Sci. Technol.* 124:35 (1997).
- Tsuji, H., and Yamaoka, I., *Proc. Combust. Inst.* 12:997 (1969).
- Tsuji, H., and Yamaoka, I., *Proc. Combust. Inst.* 13:723 (1971).
- Liñán, A., *Acta Astronaut.* 1:1007 (1974).
- Hahn, W. A., and Wendt, J. O. L., *Proc. Combust. Inst.* 18:121 (1981).
- Tsuji, H., *Prog. Energy Combust. Sci.* 8:83 (1982).
- Dixon-Lewis, G., David, T., Haskell, P. H., Fukutani, S., Jinno, H., Miller, J. A., Kee, R. J., Smooke, M. D., Peters, N., Effelsberg, E., Warnatz, J., and Behrendt, F., *Proc. Combust. Inst.* 20:1893 (1984).
- Smooke, M. D., Puri, I. K., and Seshadri, K., *Proc. Combust. Inst.* 22:1783 (1986).
- Friedman, R., footnote in Spalding, D. B., *Int. J. Heat Mass Transfer* 2:293 (1960).

12. Ablow, C. M., and Wise, H., *Solid Propellant Kinetics, II: Theoretical Analysis of the Heterogeneous Opposed Flow Diffusion Flame*, SRI report PYU 8378, 1971.
13. Inami, S. H., and Wise, H., *Solid Propellant Kinetics, III: Experimental Study of the Opposed Flow Solid Propellant Diffusion Flame*, SRI report PYU 8378, 1971.
14. Wiersma, S. J., and Wise, H., *Combust. Sci. Technol.* 19:1 (1978).
15. Mitani, T., and Niioka, T., *Proc. Combust. Inst.* 20:2043 (1984).
16. Tanoff, M. A., Ilicic, N., Smooke, M. D., Yetter, R. A., Parr, T. P., and Hanson-Parr, D. M., *Proc. Combust. Inst.* 27:2397 (1998).
17. Melton, L. A., *Appl. Opt.* 23(13):2201 (1984).
18. Wang, H., Du, D. X., Sung, C. J., and Law, C. K., *Proc. Combust. Inst.* 26:2359 (1996).
19. Dalzell, W. H., and Sarofim, A. F., *Transactions of the ASME Journal of Heat Transfer* 91:100 (1969).
20. Ermolin, N. E., Korobeinichev, O. P., Tereshchenko, A. G., and Fomin, V. M., *Combust. Exp. Shock Waves* 18:46 (1982).
21. Smooke, M. D., Crump, J., Seshadri, K., and Giovangigli, V., *Proc. Combust. Inst.* 23:463 (1990).
22. Chelliah, H. K., Law, C. K., Ueda, T., Smooke, M. D., and Williams, F. A., *Proc. Combust. Inst.* 23:503 (1990).
23. Gelbard, F., and Seinfeld, J. H., *J. Coll. Int. Sci.* 78:485 (1980).
24. Smooke, M. D., McEnally, C. S., Pfefferle, L. D., Hall, R. J., and Colket, M. B., *Combust. Flame* 117:117 (1998).
25. Hall, R. J., Smooke, M. D., and Colket, M. B., in *Physical and Chemical Aspects of Combustion: A Tribute to Irvin Glassman, Combustion Science and Technology Book Series* (R. F. Sawyer and F. L. Dryer, eds.) Gordon and Breach, Amsterdam, 1997.
26. Colket, M. B., and Hall, R. J., in *Soot Formation in Combustion, Mechanisms and Models, Springer Series in Chemical Physics, Vol. 59* (H. Bockhorn, ed.) Springer-Verlag, Heidelberg, Germany, 1994, p. 442.
27. Giovangigli, V., and Darabiha, N., "Vector Computers and Complex Chemistry Combustion" in *Proceedings of the Conference on Mathematical Modeling in Combustion*, NATO ASI Series, Lyon, France, 1987.
28. McEnally, C. S., Schaffer, A. M., Long, M. B., Pfefferle, L. D., Smooke, M. D., Colket, M. B., and Hall, R. J., *Proc. Combust. Inst.* 27:1497 (1998).
29. Parr, T. P., and Hanson-Parr, D. M., "AP Diffusion Flame Structure," in *Proceedings of the Thirty-Fourth JANNAF Combustion Subcommittee Meeting*, West Palm Beach, FL, October 1997, Vol. II, CPIA Publication 662, p. 13.

COMMENTS

Hai Wang, University of Delaware, USA. The computed soot volume fraction profile seems to be skewed toward the cold fuel jet when compared to the experimental profile. Could you comment on whether this discrepancy is caused by the uncertainty in soot transport properties or the uncertainty in soot chemistry?

Author's Reply. Brownian diffusion of soot particles is expected to be much less important than thermophoretic transport, and the thermophoretic velocities are thought to be predicted accurately. Hence, it is most likely that the discrepancy in the skewness arises from uncertainty in soot chemistry, either the gas phase chemistry affecting soot growth species, or the inception and surface growth processes. The quality of agreement shown between experiment and theory was obtained only when a surface growth model exhibiting an inverse temperature dependence at elevated temperatures was used, that is, one exhibiting the familiar bell-shaped curve in which the surface growth rises to a maximum in the vicinity of 1800 K and then declines

at higher temperatures. The particular surface growth model used is that given by Collate and Hall (1994), and it includes a process of elimination of acetylene from the soot radical at high temperatures, analogous to phenyl radical decomposition, and gives much better agreement than a simple Arrhenius-type expression for the surface growth.

•

James S. T'ien, Case Western Reserve University, USA. Have you done a sensitivity analysis of the species boundary conditions on the AP surface?

Author's Reply. Yes, we have performed a sensitivity analysis of the species boundary conditions for the AP surface. Changes in the nitrogen and chlorine species, for example, can affect the downstream flame structure. As a result, we believe that in future computations it will be critical for condensed-phase decomposition products to agree well with the corresponding surface species measurements included in Table 1 of our paper.